ISSN : 0973 - 8355

www.ijmmsa.com

INTERNATIONAL JOURNAL OF MATHEMATICAL, MODELLING, SIMULATIONS AND APPLICATIONS

IJMMSA

E-MAIL
editor.ijmmsa@gmail.com
editor@ijmmsa.com

INTERNATIONAL JOURNAL OF MATHEMATICAL, MODELLING, SIMULATIONS AND APPLICATIONS
IJMMSA

ISSN 0973-8355www.ijmmsa.com
Vol 11,Issuse 2.May 2023

ENERGY MANAGEMENT STRATEGY ADOPTING POWER TRANSFER DEVICE CONSIDERING POWER QUALITY IMPROVEMENT AND REGENERATIVE BRAKING ENERGY UTILIZATION FOR DOUBLE-MODES TRACTION SYSTEM

[1]G. RAJA LAXMI,[2]D. LAVANYA,[3]G. LAHARIKA,[4]J. MANASA

ABSTRACT

In order to cope with power quality problems and low utilization rate of regenerative braking energy (RBE) in double-modes traction system, a power transfer device integrating supercapacitor (PTDS) is proposed in this paper. A hierarchical control strategy containing an energy management layer and a converter control layer is presented, which can realize the rapid and accurate control performance. Based on the different operation states of the AC and DC traction systems, the energy management layer is divided into three working modes and ten working scenarios. The converter control layer realizes the reactive power compensation by controlling the AC-DC converter. Furthermore, by controlling the back-to-back converter in PTDS, the energy interconnection between the AC and the DC traction system is achieved. Moreover, the supercapacitor (SC), connecting at the DC bus, can store the RBE and release it to effectuate the peak clipping and valley filling. Finally, the feasibility of improving the power quality and utilizing the RBE of the proposed PTDS and its control strategy is verified.

INTRODUCTION

Several difficulties and technological constraints have arisen as a result of the rising need for dispersed generation to permit significant contributions to the grid. Substations have experienced a number of changes in design and operation to accommodate the intermittent nature of renewable power and the ever-increasing demand for electrical energy [1]. As a result of these needs, the power system has developed to include monitoring and control functions across the whole system [2]. Power electronics converters have been used to implement these features, which have had a number of positive effects on both the distribution and transmission networks [3-5]. The transmission and distribution systems may benefit from the services provided by Flexible AC Transmission Systems (FACTS), which have been shown to increase the systems' dependability, quality, and stability [9]. The UPFC is widely regarded as the most adaptable tool of its kind for relieving line congestion and expanding the capacity of already existing lines. Bulky isolation transformers, complicated multilevel topologies, or back-to-back converters handling the rated line power have traditionally been used to connect power electronics converters to offer UPFC services [10, 12].

[1]ASSISTANT PROFESSOR, [2,3&4] UG SCHOLAR
DEPARTMENT OF EEE,
MALLA REDDY ENGINEERING COLLEGE FOR WOMEN, HYDERABAD

In order to avoid using cumbersome isolation transformers, transformer-less methods using multilayer topologies have emerged as a viable alternative. However, such topologies often need a sophisticated design since they deal with the whole rated line voltage. Because of its ability to isolate the components of the power system, transformers are a practical way to connect shunt and series power electronic equipment to the grid. However, when thinking about high power compensating systems, size, cost, and footprint are all important considerations. In order to deal with these issues, recent works have shown the integration of power electronic devices into a normal transformer [13–15] or the building of a power electronics–based transformer [16]. However, these methods either only deal with one kind of compensation [13], are limited to certain applications [14–16], or are very resource-intensive and difficult to implement [16]. A distribution transformer with integrated series and shunt power electronics converters is shown in the CPAT published in [17, 18]. In the same way as a Sen Transformer [15] combines many transformers into a single unit, a CPAT does the same thing. Comparatively, a Sen Transformer has a step response, whereas a CPAT has a smoother transition between phases. This is because a CPAT has power electronics converters. Shunt services, including reactive power compensation, removal of harmonics, and reduction of inrush current, are among those given by the CPAT. A Sen Transformer can't do all of those things. While the CPAT has been studied, it has only been for single-phase uses and in the context of a UPQC in a distribution network. Since the offered auxiliary windings may be employed for any shunt-series application, the CPAT's operating principle allows for the realization of transmission applications as well. The isolation requirement may be met in a number of ways, including transformer-less systems [19, 20] and power-electronics based transformers [3-5], which have different effects on the distribution network and the transmission network. The transmission and distribution systems may benefit from the services provided by Flexible AC Transmission Systems (FACTS), which have been shown to increase the systems' dependability, quality, and stability [9]. The UPFC is widely regarded as the most adaptable tool of its kind for relieving line congestion and expanding the capacity of already existing lines. Bulky isolation transformers, complicated multilevel topologies, or back-to-back converters handling the rated line power have traditionally been used to connect power electronics converters to offer UPFC services [10, 12]. In order to avoid using cumbersome isolation transformers, transformer-less methods using multilayer topologies have emerged as a viable alternative. However, such topologies often need a sophisticated design since they deal with the whole rated line voltage. Because of its ability to isolate the components of the power system, transformers are a practical way to connect shunt and series power electronic equipment to the grid. However, when thinking about high power compensating systems, size, cost, and footprint are all important considerations. In order to deal with these issues, recent works have shown the integration of power electronic devices into a normal transformer [13–15] or the building of a power electronics–based transformer [16]. However, these methods either only deal with one kind of

compensation [13], are limited to certain applications [14–16], or are very resource-intensive and difficult to implement [16]. A distribution transformer with integrated series and shunt power electronics converters is shown in the CPAT published in [17, 18]. In the same way as a Sen Transformer [15] combines many transformers into a single unit, a CPAT does the same thing. Comparatively, a Sen Transformer has a step response, whereas a CPAT has a smoother transition between phases. This is because a CPAT has power electronics converters. Shunt services, including reactive power compensation, removal of harmonics, and reduction of inrush current, are among those given by the CPAT. A Sen Transformer can't do all of those things. While the CPAT has been studied, it has only been for single-phase uses and in the context of a UPQC in a distribution network. Since the offered auxiliary windings may be employed for any shunt-series application, the CPAT's operating principle allows for the realization of transmission applications as well. Several methods have been proposed in the literature that handle the isolation problem without using transformers [19, 20] or transformers based on power electronics.

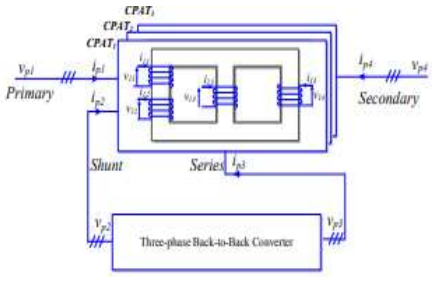

Fig. 1. Three-phase CPAT configuration using three single-phase CPATs and a back-to-back converter

B. Structuring 1. MODEL FOR A NON-LINEAR TRANSFORMER

An analogous model (Fig. 2 (a)) may be derived by discretizing the magnetic flux routes in the core (Fig. 2). m is the number of limbs, and k is the number of winding kinds, where k=1 (primary), 2 (shunt), 3 (series), and 4 (secondary) as shown in Fig. 2(a). Core linkage fluxes (cm), winding fluxes (k), leakage fluxes (Lk) per winding, and core leakage flux (0) are the several types of fluxes present in this circuit. The B-H properties of the core Material are used to determine the value of the non-linear reluctances RY and RL, which stand in for the core's limbs and yokes, respectively. In a closed-loop between input flux and output magneto-motive force (F), as illustrated in Fig. 2(b), a non-linear reluctance is modeled as a controlled magneto-motive source. Based on the limb or yoke length (l), area (A), and the core B-H characteristics given in Fig. 3, this model would generate an opposing magneto-motive force. Linear reluctances are used to depict winding leakage reluctances (Rk) and core leakage reluctances (R0). The relative permeability of air (0=410-7) is used with the flux route length and the mean area to calculate leakage reluctances. To simulate winding losses and core equivalent losses, we connect the flux produced by each winding to an electric circuit for that winding, as illustrated in Fig.2(c). Depending on the winding resistance (Rk), the equivalent core loss resistance (Rc), and the effective winding current (iek), one may calculate the equivalent transformer winding current (ik) for a given applied winding voltage (vk). As can be seen in Fig.2(c), the effective current is determined by the effective magneto-motive force (Fk) of the winding and the number of turns (Nk). From the winding electric circuit's

effective voltage (vek), the magnetic circuit's winding flux may be calculated.

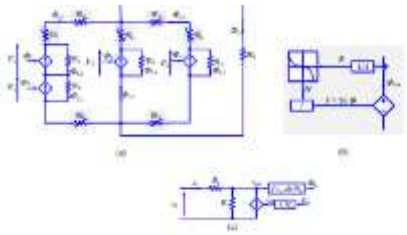

Fig. 2. Equivalent magnetic circuit model of a single-phase CPAT. (a) core equivalent magnetic circuit, (b) non-linear core reluctance model, and (c) winding equivalent electric circuit.

The Linear Transform Model, Version 2

By performing a duality translation from the magnetic circuit (Fig. 2) to its corresponding electric circuit (Fig. 3), a linear representation of the model may be obtained. The ideal couplings between the main, shunt, series, and secondary windings are predicated on the non-linear core impedances being constant and sufficiently large. The impedances of the core's magnetization (Le1, Le2, and Le3) and the resistances to the core's loss (Re1, Re2, and Re3) are denoted by Le1, Le2, and Re3, respectively. The symbols Lk and L0 denote the leakage inductances and the zero-sequence magnetizing inductances of a transformer, respectively. Besides having just one winding on each of the primary and secondary branches, the corresponding circuit (Fig. 3) is the same as that of a three-phase transformer. This circuit's characteristics may be calculated using standard transformer test procedures [24] for transient analysis at low and medium frequencies.

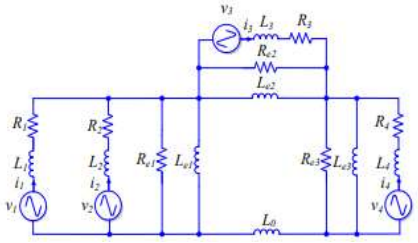

Fig. 3. Equivalent linear electric circuit of a single-phase CPAT

Modeling Power Converters 3

The structure shown in Fig.4 was used to realize the configuration shown in Fig.1. The CPAT's shunt and series windings were coupled to a three-phase back-to-back converter. The shunt converter functioned as a current controlled voltage source inverter (CCVSI) with a low-pass low-pass (LCL) filter, much like a conventional unidirectional power factor correction (UPFC). To achieve the desired level of harmonic attenuation and resonance frequency, the filter parameters L1sh, Csh, and L2sh were used. The shunt damping resistance (Rsh) proved effective in suppressing the filter's resonance. To provide the capability to inject triplen harmonic current in the shunt windings, the converter was wired in a three-phase, four-wire topology. It was clear that the transformer needed magnetizing harmonic currents. Consequently, the need for these harmonic current components on the grid might be eliminated by their injection through the shunt winding. Shunt converter current (ip2sh) is regulated by the controller, which also regulates the DC bus voltage (vdc1, vdc2) across all DC bus capacitors (Cdc). In order to offer the necessary services to the primary current (ip1), it was necessary to monitor the primary voltage (vp1) and synchronize the shunt converter voltage (vp2). In order to regulate the shunt current in accordance

with the specified reference, the shunt converter controller's output PWM signals actuated the shunt converter's converter switches. The LC filter in the series inverter was used to reduce the 3rd harmonic of the switching frequency in the output voltage (vp3), allowing the inverter to function as a voltage source inverter. Similar consideration was given to the attenuation of switching frequency harmonics and resonance damping while deciding on the filter parameters Lser, Cser, and Rser. In order to regulate the series voltage (vp3) in accordance with the services given to ip4, it was necessary to assess the secondary voltage (vp4) and current (ip4). The series inverter was driven by the series converter controller's pulse width modulated output signals to generate the target series voltage. As can be seen in Fig.4, a three-phase CPAT configuration was achieved by connecting the main, shunt, series, and secondary windings in a single CPAT core. In Fig. 5, we see a combined model of the two converters as well as the CPAT's linear model. This setup may be used to probe the CPAT's responsiveness to low- and medium-frequency transients. As can be seen in Fig. 5, the typical model disregards the impact of switching frequency harmonics by using a linearly regulated voltage source. A three-phase, three-wire converter arrangement was utilized since harmonics are ignored in this model. As shown in (2), the shunt converter power (P2) and series converter power (P3) were measured and used to simulate the common DC bus at each model sample instant (vdc).

$$v_{dc1} = v_{dc2} = -\frac{1}{2}\int \frac{P_2 + P_3}{C_{dc} v_{dc}} dt \qquad (1)$$

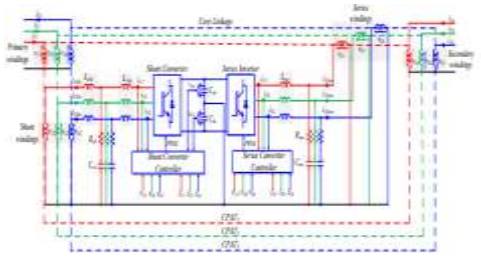

Fig. 4. Back-to-back converter topology for the three-phase CPAT.

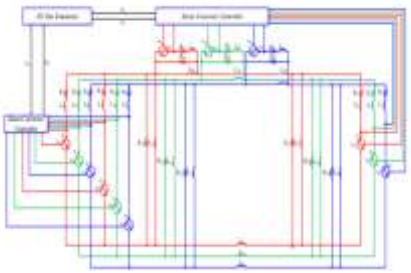

Fig. 5. Average model of the three-phase CPAT and back-to-back converter

THREE-PHASE CPAT-UPFC CONTROL

Figures 6 and 7 show the two separate controllers that make up the CPAT-UPFC's control architecture. Figure 6 depicts a shunt converter controller, the purposes of which are to eliminate harmonic components in the primary current, maintain a constant DC bus voltage relative to a reference DC bus voltage (Vdc*), and regulate reactive power through the primary relative to a reference reactive power (Q1*). For these goals, we monitor the DC bus voltages (vdc1 and vdc2), the shunt converter current (ip2), and the main grid voltage (vp1). Using the reference active (P4 *) and reactive (Q4 *) power, the series converter controller in Fig. 7 regulates the active and reactive power flowing through the CPAT's secondary winding concurrently. In addition, the load bus voltage (Vload) may be controlled to determine the value of Q4 *. Voltage at the load bus (vload), current across the load

bus (ip4), and secondary grid voltage (vp4) are the relevant control variables. Each converter has overcurrent protection for both ip2 and the series converter current (ip3). The n sample value of each measurable variable was obtained by randomly sampling measurements from each architecture using Sample and Hold. Voltages are monitored and then used by the synchronization system to calculate the equivalent frequency (), synchronizing signals (sin(t), cos(t)), magnitude (V), and synchronous reference-frame components (v, v). The analogous controller received these signals, together with the measured variables and reference variables, to calculate the appropriate modulation for the converter (M). The PWM module then calculated the corresponding switching state (g) for each switch in order to accomplish the specified control goals. The shunt controller shown in Fig.6 has been studied in [17], and its ability to meet the control goals has been demonstrated in [18]. The shunt converter current is controlled by a Proportional Resonant (PR) controller according to the desired shunt reference current (ip2 *). Both the DC bus voltage and reactive power via the primary are controlled by the fundamental component (ip2f*) of the reference, while the harmonic currents in ip1 are controlled by the harmonics component (ip2h*). A Resonant Controller set to the primary current (ip1) attenuation frequencies determines the harmonic components injected via the shunt converter. Two Proportional Integral (PI) controllers manage the DC bus voltage by maintaining a steady average DC bus voltage (vdc) and a proper distribution of DC voltages (vdc1 and vdc2). A PI controller is used to manage reactive power via the primary by determining the amount of reactive current that must be fed into the shunt converter in order to achieve the target reference Q1 *. To determine the reactive power in the feedback loop (Q1), we use (2).

$$Q_1 = \frac{1}{\sqrt{3}}\begin{bmatrix} v_{11} & v_{21} & v_{31} \end{bmatrix}\begin{bmatrix} 0 & -1 & 1 \\ 1 & 0 & -1 \\ -1 & 1 & 0 \end{bmatrix}\begin{bmatrix} i_{11} \\ i_{21} \\ i_{31} \end{bmatrix} \quad (2)$$

The series controller shown in Fig.7 includes the steps of determining the reactive power reference, determining the secondary current, and controlling the secondary current. To keep the reference load voltage (Vload*) constant, the reactive power reference (Q4 *) is set either manually or by a secondary voltage controller. Using the reference active and reactive power (P4 *, Q4 *), the secondary current calculation finds the comparable secondary current (i4, i4) in the stationary reference frame. The computations are summed up in equation (3) [25]. The i4 and i4 are converted to their three-phase equivalents (ip4 *) using the secondary synchronizing signals (sin(t)4, cos(t)4). The secondary current (ip4) is kept in step with the set point (ip4 *) by a PR controller tuned to the fundamental frequency (4). The series converter's modulation index (Mp3) is calculated by dividing the reference series voltage (vp3 *) by the DC bus voltage (vdc).

$$\begin{bmatrix} i_{\alpha 4} & i_{\beta 4} \end{bmatrix} = \frac{1}{{v_{\alpha 4}}^2 + {v_{\beta 4}}^2}\begin{bmatrix} P_4^* & Q_4^* \end{bmatrix}\begin{bmatrix} v_{\alpha 4} & -v_{\beta 4} \\ v_{\beta 4} & v_{\alpha 4} \end{bmatrix} \quad (3)$$

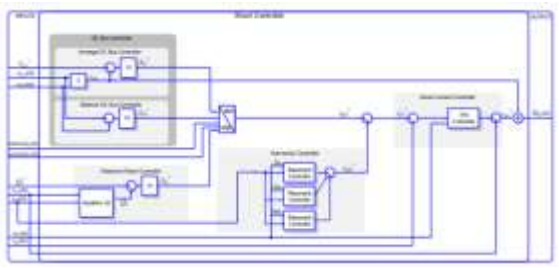

Fig. 6. Shunt Controller block structure

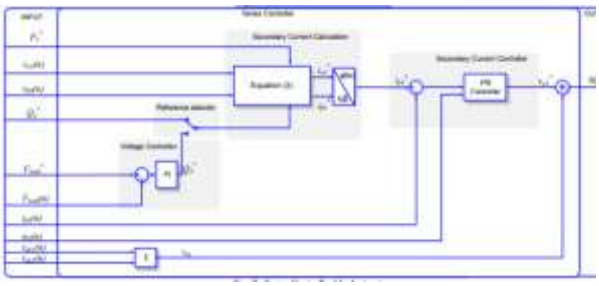

Fig. 7. Series Controller block structure.

SIMULATION OUTCOMES (IV)

Using the modeling strategy described in Section II, we modeled the CPAT setup shown in Fig. 4 using the values in Table I. The dimensions of the transformer are its limb length (lL), its yoke (lY), and its yoke area (A). As can be seen in Fig.8, the two sets of windings (primary and secondary) were linked together through a rigid grid. When the primary and secondary are activated by the same voltage, no current flows from the former to the latter. To excite the core, the CPAT would simply use the magnetizing current and split it between the two windings. At the same time, while neither shunt nor series controllers were active, neither the shunt nor the series converters injected any voltage or current. According to Fig.9, the majority of the primary current was made up of harmonics of the third, fifth, and seventh orders. Since there was no power being transferred between the primary and secondary, the majority of the primary current was made up of DC bus regulation current and the basic CPAT magnetizing current. As can be seen in Fig.10, the principal current waveform no longer contains these frequencies because of the shunt harmonics controller. Since the primary current would grow beyond the magnetizing current without being amplified, there was no need to worry about uncompensated higher-order harmonics. As can be seen in Fig.11, the shunt reactive power controller was activated with a 0 VAR reference so that the shunt converter could provide the reactive power needed by the CPAT. To modify the equivalent impedance between the main and secondary windings, the series converter delivered reactive power to the series winding (Fig. 12), and the secondary current controller was activated at a reference of 5 kW and 0 kVAR power flow. Because the secondary was injecting power into the grid, which was picked up by the main, there was an instantaneous shift in primary power as well (Fig.13). As seen in Fig.14, the DC bus controller kept the DC bus voltage stable during operation. The resulting waveform of the main and secondary currents is seen in Fig.15. Harmonics controller's ability to reduce main current harmonics at tuned frequencies is seen in the diagram.

TABLE I Parameters of the Non-linear CPAT and Converter Model

Parameter	Value
Grid voltage/phase	220V
V_{p1}, V_{p2}, V_{p3}, V_{p4}	240V, 240V, 480V,240V
I_{p1}, I_{p2}, I_{p3}, I_{p4}	70A, 7.2A, 7.2A, 70A
R_{pu}, R_{pm}	0.002 p.u., 500 p.u.
l_L, l_Y, A	0.51m, 0.3m, 0.0156 m^2
N_{p1}, N_{p2}, N_{p3}, N_{p4}	50, 50, 100, 50
V_{dc}	700V
Sampling Frequency, Switching Frequency	10kHz
C_{dc}	20mF
L_{1sh}, L_{2sh}, L_{ser}	6mH, 2mH, 7mH
R_{sh}, R_{ser}	4.7Ω, 2.35 Ω
C_{sh}, C_{ser}	5μF, 10μF

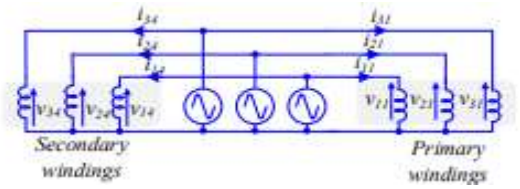

Fig. 8. Stiff grid connection to primary and secondary windings.

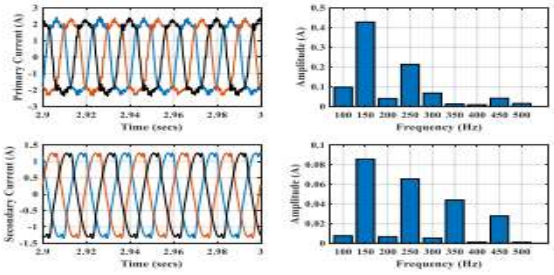

Fig.9. Primary and secondary current waveform with harmonics spectrum analysis of both currents while shunt converter disabled

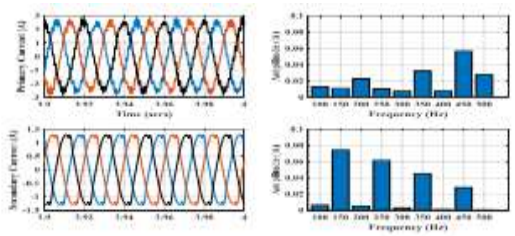

Fig. 10. Primary and secondary current waveform with harmonics spectrum analysis of both currents while shunt converter enabled.

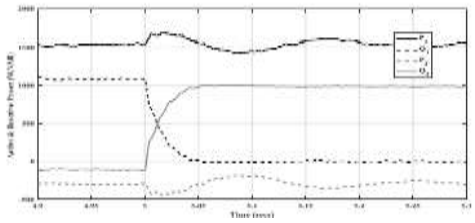

Fig. 11. Active and reactive power through the primary and shunt winding with enabled Reactive Power Controller

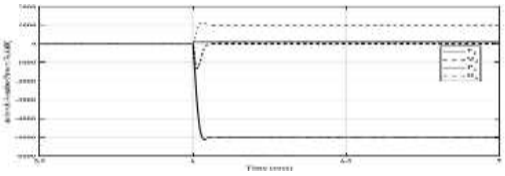

Fig. 12. Active and reactive power through the secondary and series winding during activation of the Secondary Current Controller

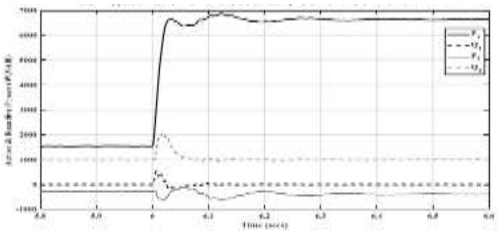

Fig. 13. Active and reactive power through the primary and shunt windings during step change in reference output power.

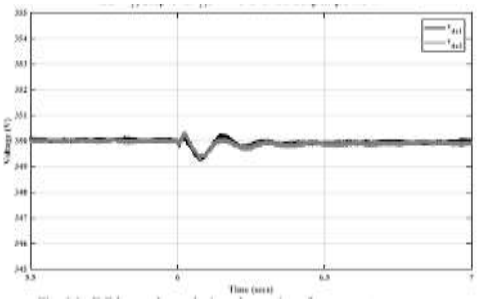

Fig. 14. DC bus voltage during change in reference output power.

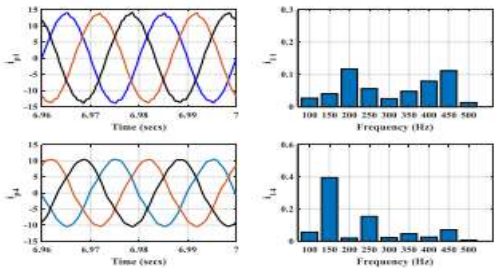

Fig. 15. Primary and secondary current waveform and harmonics spectrum with all controllers enabled.

V. RESULTS OF EXPERIMENTS

Three multi-winding three-phase transformers and two 5-kW back-to-back converters were connected in the arrangement illustrated in Fig. 16 to create the laboratory setup. In Table I, we can see all of the transformer settings. Following the layout of Fig.8, the main and secondary windings were joined together. A DS1103 controller board was used to sample and switch at a rate of 10kHz for each converter. The CPAT was implemented in an OPALRT real-time simulation case study of a 5-bus power

system to examine its functionality in a power system, as illustrated in Fig. 17. Two machines, G1 and G2, were used in the case study setup, with ratings of 1000MVA and 1200MVA, respectively. The CPAT replaced a 1000MVA step-up transformer on the 50 km transmission line from the generation bus (B1) to the transmission bus (B3), and it was installed between the two buses. Using the corresponding values listed in Table II, the CPAT was modeled after the configuration illustrated in Fig. 5. The series winding of the CPAT-UPFC was used to manage active power over the 50 km transmission line and maintain a constant load bus voltage (Vload) in this setup. To accommodate for communication latency, a 100msec lag in the observed load bus voltage was used since the CPAT-UPFC was not connected at the load bus [26]. The CPAT's shunt winding also controlled the amount of reactive power absorbed between busses B1 and B3. Bus B5 was unexpectedly linked to a 500 MW, 750 MVAR load so that the CPAT's ability to control the voltage on the bus and the electricity going into the system could be tested.

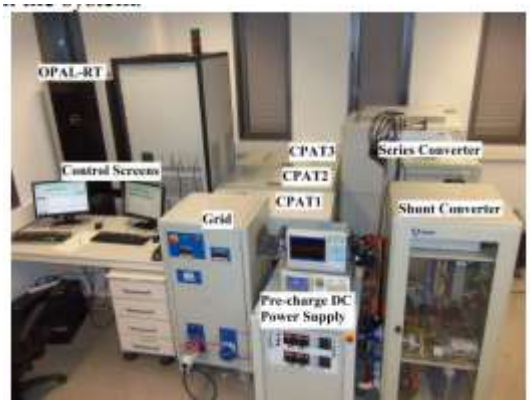

Fig. 16. Laboratory setup layout of the three-phase CPAT-UPFC

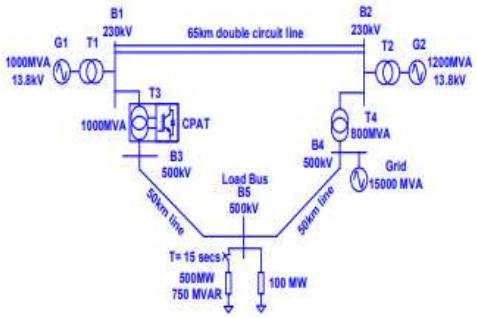

Fig. 17. Single-line diagram of 5-bus power system case study with a threephase CPAT model

TABLE II
Parameters of the Average CPAT and Converter Model

Parameter	Value
Rated Power/CPAT	333MVA
V_{p1}, V_{p2}, V_{p3}, V_{p4}	138.5kV, 138.5kV, 138.5kV,288.6kV
R_{ph}, R_{epm}	0.002 p.u., 500 p.u.
L_{ph}, L_{epm}, L_0	0.002 p.u., 500 p.u., 0.003 p.u.
V_{dc1}, V_{dc2}	250kV
Control sampling frequency	10kHz

Stiff grid

The DC bus controller was turned on at the beginning of setup to provide a stable DC supply throughout the process. As can be seen in Fig. 18(a), under this condition, the majority of the primary current's harmonic spectrum was made up of 3rd and 5th -order harmonics, with a magnitude of 55% and 18%, respectively. Two percent of the magnetizing current came from the 2nd and 7th -order harmonics. Harmonics in the main current were decreased by more than 95% when the harmonics controller was set to third, fifth, and seventh -order frequencies (Fig. 18 (b)). As can be seen in Fig. 19, the reactive power compensation controller was adjusted to eliminate all reactive power in the primary. At that precise moment, the current through the shunt windings rose, allowing the shunt converter to provide the necessary 1.8 kVAR from the primary. The 1.8 kVAR magnetizing power of the CPAT. The shunt converter provided the reactive power for the secondary winding and

CPAT at steady state. In order to feed an additional 5 kW into the grid from the primary, the series converter was programmed with a -5kW reference for the secondary. As can be seen in Fig. 20, when the secondary current controller was activated using the reference value, the secondary current rose, providing the necessary amount of output power. To alter the power flow in the transformer by 10% of its rated power, the series converter primarily provided reactive power, requiring around 25% of the rated converter power. Simultaneously, the active power demanded by the secondary winding and transformer core was met by a rise in the main current (Fig. 21). In addition, the shunt converter used an additional 570 W to keep the DC bus voltage stable while delivering the active power required by the series converter.

System of 5 Power Buses The OPAL-RT was used to run a real-time simulation of the 5-bus power system so that we could examine the power system's stability when the CPAT was active. The impact of a sudden load connection on the CPAT-UPFC system's functioning, both with and without compensation, was analyzed (Fig. 17). Before making the load connection, P4*=330MW, Q4*=-30MVAR, Q1*=-25MVAR, Vload=500kV, and vdc*=500kV were established as the nominal power-flow values. After these baselines were established, system behavior was compared to that of a system without a CPATUPFC controller (i.e., both shunt and series converters turned off). What happens to the power sources in the system when loads are connected is shown in Fig.22. Significant damping on G1 was seen from the CPAT (Fig.22(a)), which moved the oscillations to G2 and the grid. Since the CPAT delivered most of the reactive power (Fig.22(b)) needed to compensate for the load voltage drop, G1's reactive power needs were lowered. The shunt converter (Q2 in Fig.22(b)) greatly decreased the reactive power flowing through the primary winding of the transformer. The shunt converter was also responsible for meeting the higher reactive power need at the load bus. The series converter controller allowed for active power dampening in both the primary and secondary stages, as illustrated in Fig.22(b). The series converter action (P3 in Fig.22(b)) absorbed active power at the time of load connection, demonstrating the damping effect. Later, when the secondary power reference had to be kept constant, the series converter provided the active and reactive power needed to do so. In Fig.23, we see how the regulation affects the load bus voltage and DC bus voltage when the load is connected. The load voltage oscillation was less damped due to the delay in communication. However, the CPAT made up for the 5% loss in voltage at the load bus. The impact of voltage controller tuning on delay-in-communication responses was not explored. Because the series converter originally sucked in active power (P3 in Fig.22(b)), the DC bus voltage rose during the load connection, as indicated in Fig.23. When the shunt converter took in active power and delivered reactive power into the grid, as shown in Fig.22(b), the DC bus would recharge to keep the voltage stable, as shown in Fig.23.

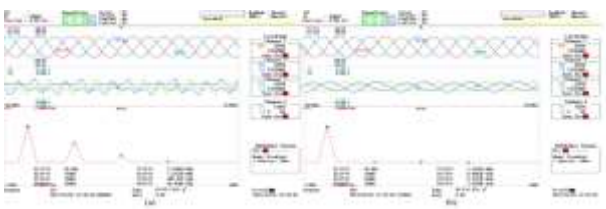

Fig. 18. Experimental primary current waveform and harmonics spectrum. (a) without harmonics compensation and (b) with harmonics compensation.

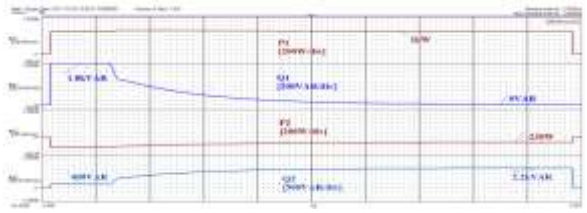

Fig. 19. Experimental results of shunt converter operation with Reactive Power Compensator controller set to 0kVAR (200ms/div)

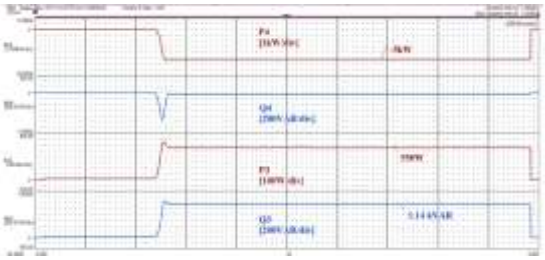

Fig. 20. Experimental results of series converter operation with Secondary Current Controller set to -5kW (200msec/div).

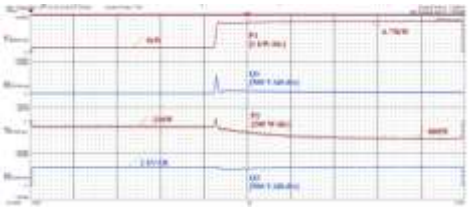

Fig. 21. Experimental results of primary and shunt winding power during activation of Secondary Current Controller set to -5kW(200ms/div).

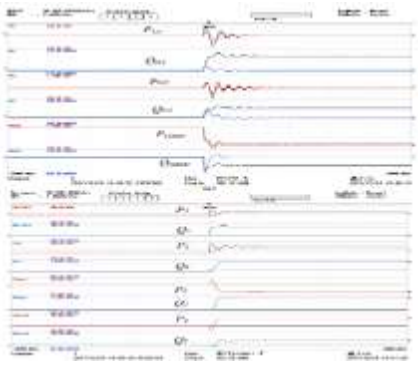

Fig. 22. Real-time simulation of the active and reactive power through the 5-bus power system with controllers disabled (black lines) and controllers enabled. (a) Grid sources and (b) CPAT windings (2sec/div).

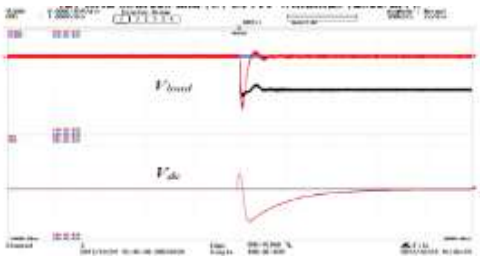

Fig. 23. Real-time simulation of the load voltage and DC bus voltage during load connection with controllers disabled (black line) and with controllers enabled.

CONCLUSION

Using three CPATs in series and a back-to-back converter, this work introduces the CPAT-UPFC. Multiple grid functions, such as the removal of harmonic currents, reactive power compensation, and power flow regulation, are made possible by a CPAT's combination of shunt and series windings. Under stiff-grid operation and in a 5-bus power system model, a CPAT's linear and non-linear modeling methodologies have been presented and explored. Simulations and an experimental prototype have been used to assess the effectiveness of the provided control architecture in enabling a CPAT to function as a UPFC. The analytical, modeling, and experimental findings all corroborate CPAT-UPFC's competency in this regard. VIII.

SOURCES CITED

1."Review of microgrid architectures - a system of systems perspective," published in IET Renewable Power Generation, vol. 9, no. 8, pp. 1064-1078, November 2015. "Smart Substation: State of the Art and Future Development,"

2.Q. Huang, S. Jing, J. Li, D. Cai, J. Wu, and W. Zhen, IEEE Trans. Power Del., vol. 32, no. 2, pp. 1098-1105, Apr. 2017. IET Generation, Transmission &

Distribution, volume 11:issue 5:pages 1202-1211, March 2017

3.H. Liao and J. V. Milanovi, "On capability of different FACTS devices to mitigate a range of power quality phenomena," "Toward Power Quality Management in Hybrid AC-DC Microgrid Using LTC-L Utility Interactive Inverter: Load Voltage-Grid Current Tradeoff,"

4.M. Shahparasti, M. Mohamadian, P. T. Baboli, and A. Yazdianp. Pages 857–867 in IEEE Transactions on Smart Grid, Issue 2 (March 2017).

5. "Integration of Distributed Generation in the Volt/VAR Management System for Active Distribution Networks," by J. Barr and R. Majumder, IEEE Trans. Smart Grid, volume 6, issue 2, pages 576-586, March 2015.

6."All Nodes Voltage Regulation and Line Loss Minimization in Loop Distribution Systems Using UPFC," by M. A. Sayed and T. Takeshita, published in IEEE Trans. Power Electron., vol. 26, no. 6, pp. 1694-1703, June 2011.